M-sequences in ophthalmic electrophysiology

Philipp L. Müller

Department of Ophthalmology, University of Bonn, Bonn, Germany

Thomas Meigen

Dr. Thomas Meigen Smart Solutions, Würzburg, Germany
Department of Ophthalmology, University of Würzburg, Wüzburg, Germany

The aim of this review is to use the multimedia aspects of a purely digital online publication to explain and illustrate the highly capable technique of m-sequences in multifocal ophthalmic electrophysiology. M-sequences have been successfully applied in clinical routines during the past 20 years. However, the underlying mathematical rationale is often daunting. These mathematical properties of m-sequences allow one not only to separate the responses from different fields but also to analyze adaptational effects and impacts of former events. By explaining the history, the formation, and the different aspects of application, a better comprehension of the technique is intended. With this review we aim to clarify the opportunities of m-sequences in order to motivate scientists to use m-sequences in their future research.

Introduction

The clinical routine as well as research of human physiology are increasingly dominated by diagnostic investigation. Imaging techniques are distinguished from laboratory and functional testing. Diagnostic investigation helps in objectifying medical conditions. However, the use of functional testing in the field of neurology and ophthalmology is limited because a minimum of attention, volition, and cognitive capability is required. Therefore, objective functional testing has entered the clinical workup, especially electrophysiology.

Ophthalmic electrophysiology has become an irreplaceable diagnostic tool in neurologic and ophthalmologic clinical routines. Electroretinogram (ERG) and visual evoked potential (VEP) are used in particular. These highly objective methods not only indicate the disease-causing alterations but also provide the ability to estimate possible progression in some cases. However, ERG and VEP are limited in their topographic value. No statement can be made regarding the location of a lesion using full-field ERG or VEP. This problem was solved by multifocal techniques. Indeed, the multifocal ERG (mfERG) and VEP (mfVEP) allow a simultaneous recording of evoked responses from a large number of regions within the visual field. The multifocal techniques usually are based on specific sequences for stimulation called *maximal length shift-register sequences* or *m-sequences*, first applied to this scope by Sutter and colleagues.

The mathematical properties of m-sequences allow for the separation of responses generated within multiple visual field locations. Moreover, the use of binary m-sequences enables one to analyze adaptational effects and impacts of former events. As a result, the multifocal technique is currently expanding from experimental to clinical application and enables visual scientists to investigate and characterize the visual system.

During the past 20 years, m-sequences have successfully been applied in clinical routine. As the underlying mathematical rationale is often daunting, a pragmatic "black box" approach is chosen in many clinical settings where the responses of the visual system to a wildly flickering stimulus pattern are related to signals from different parts of the visual field by some "magic machine." The aim of this review is to use the multimedia aspects of a purely digital online publication to explain and illustrate the highly capable technique of m-sequences in multifocal ophthalmic electrophysiology.

From our point of view, the use of m-sequences could offer much more diagnostic power than is currently applied in the clinical routine. Moreover, basic research on spatial and temporal interactions in the visual system might benefit from this m-sequence approach because the analysis of different kernel orders allows one to quantify the linear and nonlinear aspects of visual perception. We hope that an explanation of the m-sequence approach by multimedia elements will

Citation: Müller, P. L., & Meigen, T. (2016). M-sequences in ophthalmic electrophysiology. *Journal of Vision*, *16*(1):15, 1 19, doi:10.1167/16.1.15.

doi: 10.1167/16.1.15 Received April 23, 2015; published January 27, 2016 ISSN 1534-7362

help a broader audience of clinicians and researchers gain an intuitive understanding of the formation, analysis, and capabilities of m-sequences. After the methodological aspects have been introduced by educational movies and graphics, the article reviews the current application of the m-sequence technique in clinical routine and basic research and points to possible applications in the future. Each educational movie is provided as supplementary material and is referenced by a hyperlink below a static image that represents a typical moment within the movie.

History of m-sequences

Zierler (1959) set the mathematical background of m-sequences describing linear recurring sequences. Further publications revealed the potency of binary m-sequence (i.e., in the construction of test inputs; Davies, 1970; Golomb, 1982; Kruth, 1981; MacWilliams & Sloane, 1977; Marmarelis & Marmarelis, 1978; Zierler, 1968). Also, m-sequences with more than two states, such as ternary m-sequences, have been introduced (Citron, Emerson, & Wollmann, 1983; Moller, 1983; Ream, 1967). It took several years until binary m-sequences were introduced into ophthalmic electrophysiology. In 1975 and 1979 they were first applied for ERG measurements (Fricker & Sanders, 1975; Larkin, Klein, Ogden, & Fender, 1979), and in 1993 m-sequences were used for the first time as a method to produce VEP stimulation (Collins & Sawhney, 1993). The application of this strategy was shown to improve signal-to-noise ratio and to reduce the recording times compared with former approaches (Fricker & Sanders, 1975; Srebro & Wright, 1998). Sutter and colleagues (Sutter, 1988; Sutter & Tran, 1992) created a multifocal stimulation mode based on m-sequences. Using this technique it was possible to examine several independent visual fields with only a single stimulation series, enabling objective topographic mapping of retinal and cortical function. Subsequently, m-sequences have been applied by other groups to solve a growing number of problems. mfERG and mfVEP have entered clinical routine as irreplaceable diagnostic tools (Betsuin, Mashima, Ohde, Inoue, & Oguchi, 2001; Lai et al., 2007). By now, various commercial systems have become available. To enable comparable results, guidelines for mfERG recordings were first published in 2003 by the International Society for Clinical Electrophysiology of Vision (Marmor et al., 2003). In 2012, a standard for mfERG was released (Hood et al., 2012). To date, no guidelines for mfVEP have been published by the International Society for Clinical Electrophysiology of Vision. Consequently, investigators must be aware of different mfVEP settings used by the various systems.

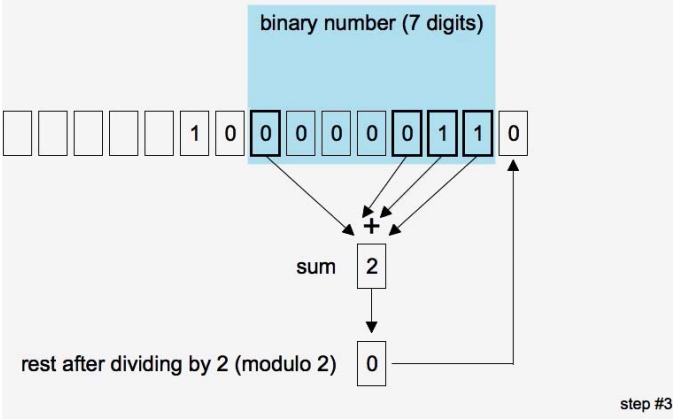

Figure 1. Generation of m-sequences. The generation of m-sequences starts with a shift register consisting of a specific number of digits (here seven) holding the states *1* or *0*. The modulo 2 sum (parity) of a specific subset of this shift register (here the first and the last three digits; bold rectangles) is fed back into the serial input. In the first step the sum of the chosen digits is even, resulting in a *0* positioned at the end of the shift register. After shifting the sequence by one digit each time, the following steps are created in the same way. The chosen subset of the shift register is appropriate for generating a maximum length shift register sequence (m-sequence) because the initial content does not repeat before the maximum possible number of $2^n - 1 = 2^7 - 1 = 127$ steps. (The full movie associated with this figure can be found in the Supplemental data section.)

Generation of m-sequences

The mathematical foundation of m-sequence stimulation has been described in many publications since its introduction into ophthalmic electrophysiology (Baseler, Sutter, Klein, & Carney, 1994; Davies, 1970; Kruth, 1981; MacWilliams & Sloane, 1977; Sutter, 1988; Sutter & Tran, 1992; Zierler, 1959). An m-sequence is a binary series of two states (*1* and *0*). M-sequences are pseudorandom in the sense that they seem random but follow a strict generation rule using digital shift registers with a linear feedback (Golomb, 1982; Keating & Parks, 2006; Marmarelis & Marmarelis, 1978; Sutter & Tran, 1992). The following section describes this specific generation of pseudorandom binary m-sequences by means of Movie 1 (Figure 1). The generation of m-sequences starts with a shift register consisting of a definite number of digits ($n = 7$ in Movie 1) holding the states *1* or *0* (initially often called *seed*). The modulo 2 sum (parity) of a specific subset of this shift register (tap register) is fed back into the serial input. In the present example (Movie 1), the first and the last three digits were chosen for this subset (bold rectangles). The modulo 2 sum represents the rest after dividing the sum of the chosen digits by 2. If the sum is even, the rest after division by 2 is *0* (first step of

Movie 1). If it is odd, the formula results in *1*. The resulting digit is positioned at the end of the binary number representing a new step (linear feedback). After shifting the sequence by one digit each time, the following steps are created in the same way (digital shift registers). Depending on the length of the shift register and the chosen subset to be fed back, the content of the shift register will recur and the sequence repeats at a specific point. The longest possible sequence has the maximal length of $2^n - 1$ steps before it repeats, meaning that each of the possible $2^n - 1$ arrangements of *1* and *0* can be found somewhere in the sequence. Consequently, generated sequences with a length of $2^n - 1$ steps (in our example, $2^7 - 1 = 127$) are referred to as *maximum length feedback shift register sequences* or simply *binary m-sequences* (Sutter & Tran, 1992). The only missing arrangement from all possible 2^n configurations is the zero state (i.e., all digits in the register are *0*). The zero state is a cycle in itself as the respective modulo 2 sum always results in *0*.

It is important to keep in mind that not every subset (tap register) leads to a suitable m-sequence. If an arbitrary subset is chosen it is very likely that the content of the shift register repeats before the maximum number of $2^n - 1$ steps is reached. In this case the resulting stimulation sequence would depend on the initial values of *0*s and *1*s within the shift register (often called *seed*). Moreover, the repetition of parts of the sequence is a correlation that can lead to a cross-contamination (also known as *cross-talk*) of responses from different parts of the visual field when different fields are stimulated with shifted versions of the same sequence (Ireland, Keating, Hoggar, & Parks, 2002; Keating & Parks, 2006). Thus, it is mandatory to ensure that a subset is chosen that generates sequences with a length of $2^n - 1$ steps regardless of the initial seed.

Cross-correlation

Cross-correlation in the present setting represents the summation of all products of each shifted version of a sequence with the original sequence (Sutter & Tran, 1992). Using this mathematical procedure, specific characteristics of m-sequences can be demonstrated. In order to avoid multiplication with 0, nomenclature of the m-sequence steps has to be modulated. By regarding *1* as **1** and the opposite state *0* as **−1**, the mathematical properties are preserved because the multiplication of the elements **1** and **−1** is equivalent to a modulo 2 sum of the elements *0* and *1* using this substitution.

The stepwise product of an unshifted m-sequence with itself (first and second cylinders in the first part of Movie 2; Figure 2) reveals a series of sole **1**s ($\mathbf{1} \times \mathbf{1} = \mathbf{1}$ and $\mathbf{-1} \times \mathbf{-1} = \mathbf{1}$; third cylinder in the first part of Movie 2). The sum of this series has the value $2^n - 1$ (in our example, $2^7 - 1 = 127$), implying maximum correlation.

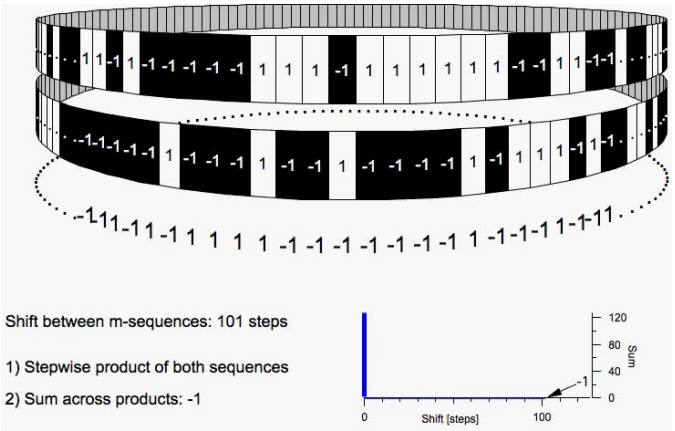

Figure 2. Cross-correlation. The first part of the movie shows two cylinders carrying the very same m-sequence without shifts. A correlation between the original m-sequence and all possible shifted versions of the m-sequence (second part of the movie) is calculated in the following way. First, a stepwise multiplication (highlighted in blue) is performed. Then the 127 products are added and the resulting correlation value is displayed in the bottom right diagram as a function of the shift between the two m-sequences. In the second part of the movie the stepwise multiplication is displayed in an accelerated way in only one step. For a shift of zero steps a maximal correlation of 127 is achieved. The correlation between all 126 other shifted versions of the m-sequence and the original m-sequence results in the value of **−1**, implying a minimal correlation. This mutual independence of all shifted versions of the m-sequence allows one to separate the electrophysiological response of different stimulation fields (Figure 3) as well as responses from different higher order kernels (Figures 4 through 8). (The full movie associated with this figure can be found in the Supplemental data section.)

The stepwise product of identical but shifted m-sequences (first and second cylinders in the second part of Movie 2) results in new series consisting of **1**s and **−1**s (third cylinder in the second part of Movie 2). Due to the mathematical properties of m-sequences, these new series represent differently shifted versions of the original m-sequence. The sum of all **1**s and **−1**s within the m-sequence of each new series has the value of **−1** (bottom right in the second part of Movie 2), implying a minimum correlation between shifted versions of an identical m-sequence (linear independence; Sutter, 1987, 2001; Sutter & Tran, 1992).

M-sequence–based stimulation

Binary m-sequences are used as a basis for the stimulation sequence. When applied to an electro-

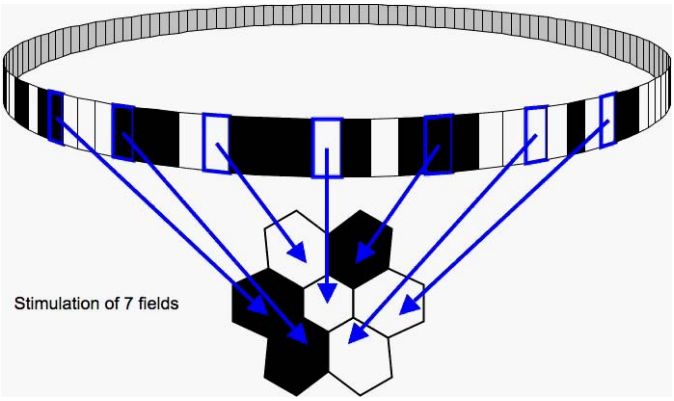

Figure 3. M-sequence–based stimulation. Binary m-sequences are used as the basis for the stimulation sequence. Stimulations are coded white, and pauses are coded black. The first part of the movie demonstrates a monofocal stimulation. One starting point in the m-sequence (highlighted in blue) is chosen to represent the single field. Whenever the m-sequence shows a pause (black square) at the respective point, the field is black as well. Proceeding the m-sequence, stimulations and pauses alternate in the stimulation field corresponding to the m-sequence. The second part of the movie focuses on multifocal stimulation in the case of seven exemplary fields. Because each field has a different starting point within the same m-sequence, its stimulation is performed independently from all other fields, which allows one to separate the responses from different fields by cross-correlation (Figure 2). (The full movie associated with this figure can be found in the Supplemental data section.)

physiological recording, a **1** represents a stimulation, whereas a **0** stands for a pause (step without stimulation). When cycling through the m-sequence, stimulations and pauses alternate corresponding to the m-sequence (first part of Movie 3; Figure 3; respective step highlighted in blue).

Due to their formation, m-sequences are linear independent to shifts (cf. Cross-correlation). Using different starting points within an identical m-sequence enables one to simultaneously and independently stimulate different fields (Baseler et al., 1994; Sutter, 1988; Sutter & Tran, 1992; Zierler, 1959). The second part of Movie 3 (Figure 3) shows a practical application in the case of seven fields. Each field has its own starting point (highlighted in blue) in the same m-sequence providing simultaneous and independent stimulation. An increasing number of investigated fields can either aggrandize the tested visual field by adding further fields at the edges or improve the spatial resolution by downsizing the fields within the existing borders (Balachandran, Klistorner, & Graham, 2003; Heinemann-Vernaleken, Palmowski, Allgayer, & Ruprecht, 2001; Kretschmann, Bock, Gockeln, & Zrenner, 2000; Zhang, Hood, Chen, & Hong, 2002). However, stimulation with smaller fields might lengthen the recording duration by decreasing signal-to-noise ratio compared with bigger stimulation fields (Balachandran et al., 2003; Heinemann-Vernaleken et al., 2001; Hood et al., 2000, 2004; Kalpadakis & Rudolph, 2003; Zhang et al., 2002). Consequently, a good balance between spatial resolution and recording duration should be chosen. To produce approximately equal-sized mfERG responses from individuals with normal retinal function, a scaling of the stimulation fields is recommended (Hood, Odel, Chen, & Winn, 2003; Hood et al., 2012; Sutter & Tran, 1992). However, the conventional scaling of the mfVEP complies with the cortical magnification of the central visual field (Baseler et al., 1994; Hood, Odel, & Winn, 2003a; Horton & Hoyt, 1991).

Theoretically, up to $2^n - 1$ independent fields can be stimulated with the same m-sequence because $2^n - 1$ different starting points are possible. But the duration of an evoked response has to be considered. In the second part of Movie 3 we chose a response waveform with a length of four steps in time. If the temporal delay between different stimulation fields was less than four steps, then the corresponding waveforms of these fields would always be superimposed in the same way and could not be separated by any data analysis procedure. This would result in a cross-contamination between different stimulus locations (Keating & Parks, 2006). As a consequence, the number of independent fields for an m-sequence with $2^n - 1$ steps depends on the length of the evoked response. A longer response leads to a smaller number of independent fields.

Binary m-sequences are used in flash as well as pattern stimulation settings. Concerning flash stimulation, **1**s represent the flash and **0**s typify pauses (Sutter, 2000, 2001; Sutter & Tran, 1992). In pattern stimulation the **1**s and **0**s are usually bound to two different stimulus patterns; for example, they represent the checkerboard (**1**) and the gray background (**0**) in pattern onset studies or the checkerboard (**1**) and the reversed checkerboard (**0**) in pattern reversal studies (Baseler et al., 1994; Hoffmann, Straube, & Bach, 2003; Hood et al., 2003a; Unterlauft & Meigen, 2008).

First-order kernel

The m-sequence approach has been very successful because it allows one to simultaneously record signals from different parts of the visual field. When responses are triggered by applying the same but shifted pseudorandom binary m-sequence for different stimulus fields (as demonstrated in Movie 3; Figure 3), the responses may overlap and it may seem difficult to isolate the individual responses. The solution to this problem is cross-correlation. We introduced the con-

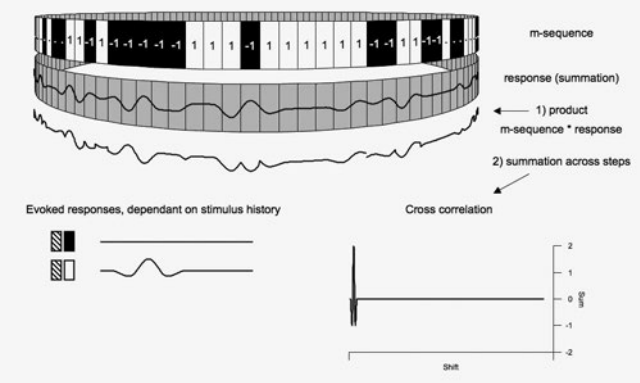

Figure 4. First-order kernel. The movie demonstrates the data analysis for a case where the response to stimulus does not depend on earlier stimulation but rather only on the current stimulation. The top cylinder shows the m-sequence stimulation by white and black rectangles. In the bottom left part, possible evoked responses for different situations are shown. White rectangles symbolize a stimulation, whereas black rectangles stand for pauses. The previous stimulation history (striped rectangles) has no effect on the current response. When the current step is black, no significant response is evoked. When the current step is white, a characteristic waveform is evoked. At each time point, the regarded step is highlighted blue and the respective evoked potentials are added in the second cylinder. The evoked potentials in the second cylinder overlap because the response is longer than the time gap between subsequent stimulation steps forming a response summation (bottom of second cylinder). In the second part of the movies, a cross-correlation between the response summation and the m-sequence is performed. The cross-correlation (see Figure 2) reveals the first-order kernel as a mean response to stimulation (bottom right). When displayed with the same temporal resolution, the waveform of the first-order kernel is identical to the single evoked response at the bottom left (see Figure 8). (The full movie associated with this figure can be found in the Supplemental data section.)

cept of cross-correlation before to show the linear independence of shifted versions of the original m-sequence (Figure 2), but the same concept can be used for data analysis (Sutter, 2001; Sutter & Tran, 1992). For this purpose a correlation between the m-sequence and recorded data is calculated for each possible shift of the stimulus sequence.

This analysis procedure is illustrated in Movie 4 (Figure 4). In the first part of Movie 4 the summed response is generated and then subjected to a cross-correlation with the m-sequence in the second part of Movie 4 for data analysis. This example shows the simplest situation where the response depends only on the current stimulation (blue rectangle). The top cylinder in Movie 4 shows the m-sequence stimulation by white and black rectangles. In the bottom left part of the movie the two options are shown. Whenever the m-sequence based stimulation arrives at a step with stimulation (white rectangle), a characteristic waveform (blue trace) is evoked, which adds to the response summation across subsequent stimulation steps. At a step without stimulation (black rectangle), no significant response is evoked; a flat waveform is added to the bottom cylinder and the summed response remains unchanged. The striped rectangle in the bottom left part indicates that the prestimulus history be it a stimulation or a nonstimulation has no effect on the current response.

The second half of Movie 4 shows how the response to a single stimulus can be estimated from the recorded mass potential by cross-correlation. For a given shift, a **1** in the m-sequence adds the recorded data while a **1** subtracts the corresponding part of the recorded data. Finally, an average across all steps of the m-sequence results in a mean response to a specific shift. The cross-correlation is a concatenation of these mean responses for all possible shifts. This calculation can be accelerated by the fast m-transform presented by Sutter and Tran (1992). The waveform at the beginning of this cross-correlation trace (bottom right at the end of Movie 4) is identical to the response to a single stimulation (bottom left part of Movie 4), which can be better seen when both traces are displayed with the same temporal resolution (summary in Figure 9, first column).

The response of a stimulation field may show deflections for a longer time than one step. In our example (Movie 4) it took more than four steps in time until the responses got back to zero level (blue traces as response to a stimulation). However, when real-world signals are recorded (e.g., in an mfVEP), it may take about 100 ms until the major cortical component (P100) develops, and there may be later response components that last more than 300 ms after visual stimulation (Odom et al., 2009). For these situations a shift of only three steps between different stimulation fields would be much too short and the responses from different stimulus fields would overlap in the cross-correlation responses (cross-contamination; Keating & Parks, 2006). In order to plan the time shifts of different stimulus fields for an m-sequence experiment, it is important to know the time course of the specific evoked response in advance.

Second-order kernel, first slice

In Movie 4 the signals did not depend in any way on the prestimulus history. But what if the neuronal processing of the stimulation would show some adaptational effects where the response to a stimulus

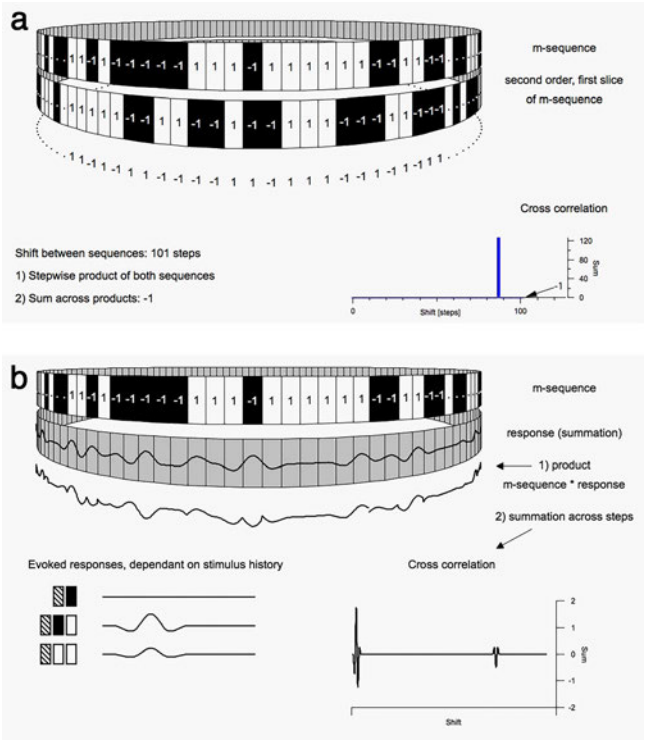

Figure 5. First slice of the second-order kernel. The movies demonstrate (a) the interaction in the processing of two subsequent stimulation steps and (b) the corresponding data analysis. As in Figure 2, the top cylinder shows the m-sequence. (a) In the first part of the movie, the product of two consecutive stimulation steps (highlighted in blue) is placed in the bottom cylinder. Continuing along the m-sequence, the stepwise products fill the bottom cylinder. In the second half of the movie, a cross-correlation between both sequences is performed. Because a maximum correlation (127) is found for a shift of 87 steps and because all other shifts show the same minimal correlation ($-\mathbf{1}$), the sequence in the second cylinder is identical to the original m-sequence but shifted by 87 steps (see Figure 2). (b) Similar to Figure 4, the bottom left part of the movie shows possible options of evoked potentials that depend on two subsequent stimulations. In this example we chose to reduce the response amplitude when a stimulation directly followed another stimulation compared with a stimulation after a pause. The superposition of the responses from subsequent stimulations and the cross-correlation analysis is identical to Figure 4. The temporal interaction between subsequent stimulations leads to an additional component starting at 87 steps in the cross-correlation result (first slice of the second-order kernel). (The full movie associated with this figure can be found in the Supplemental data section.)

would be modulated by a similar stimulation that had been processed directly before the current stimulation? Then the same stimulation would lead to a collection of different responses and the cross-correlation result so far would show only the average responses across all these response variants.

Luckily, m-sequence stimulation allows one to quantify such temporal interaction as well. Moreover, the effect of such interactions can be seen in the same cross-correlation result by *higher order kernels* without any additional data analysis (Nemoto, Momose, Kiyosawa, Mori, & Mochizuki, 2004; Sutter, 2000, 2001). Further mathematical details of kernel analysis can be found in respective publications (Klein, 1992; Voltera, 1959; Wiener, 1958).

Movie 5a (Figure 5) shows the easiest case where we want to quantify the interaction in the processing of two subsequent stimulation steps, which is called the *first slice of the second-order kernel*. The top cylinder shows the m-sequence, and the two blue rectangles indicate two subsequent stimulation steps. The bottom cylinder shows the product of the multiplication between the two stimulation steps (e.g., $\mathbf{1} \times \mathbf{1} = \mathbf{1}$) for the current steps. As the movie progresses in time, a corresponding correlation of two neighboring steps is calculated and the results fill the bottom cylinder in the first half of the movie. While this operation may seem trivial, the important aspect is shown in the second half of the movie. When we calculate the cross-correlation between the sequences of the two cylinders similar to Movie 2, a maximum correlation (127) is found for a shift of 87 steps where all other shifts show the same minimal correlation ($-\mathbf{1}$). The simple explanation of this result is that the time course of the first slice of the second-order kernel is exactly identical to the original m-sequence but shifted by a specific number of steps in this case, 87 steps.

Movie 5b (Figure 5) illustrates the consequences of such temporal interactions on recorded data and on the cross-correlation results. Again, without stimulation (black rectangle) no significant response is evoked (flat waveform), independent from the prestimulation history. However, when visual stimulation is applied (white rectangle), the response is smaller when the field was stimulated in the preceding step (two white rectangles in the bottom left part of Movie 5b) than when there was no stimulation in the preceding step (black and white rectangle in the bottom left part of Movie 5b). During the first part of Movie 5b the corresponding responses are superimposed for all steps of the m-sequence stimulation. In this case, however, the cross-correlation at the end of Movie 5b indicates a significant second-order kernel response (first slice). This second-order response appears with a delay of exactly 87 steps after the first-order response, as expected from Movie 5a.

In the example presented in Movie 5 we illustrate adaptational effects by changes in signal amplitude. However, much of the effect of fast adaptation is in the temporal domain (i.e., local response implicit time changes), whereas only some of the effect is in the amplitude domain (Sutter, 2000, 2001). This is why actual second-order kernel waveforms do not look like small, inverted first-order waveforms. We chose am-

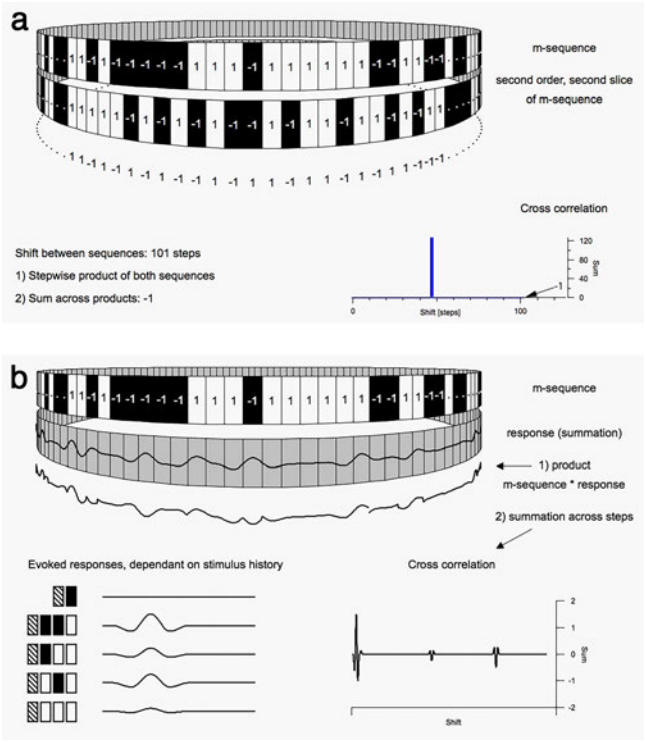

Figure 6. Second slice of the second-order kernel. The movies demonstrate (a) the interaction in the processing of two stimulation steps with a distance of two steps and (b) the corresponding data analysis. (a) The general properties are similar to those of the first slice of the second-order kernel (Figure 5). In this case, however, the multiplication is done between two observed points in time (blue rectangles) that are two steps apart. The cross-correlation shows that this temporal interaction corresponds to the same m-sequence but shifted by 47 steps. (b) The first part of the movie shows the superposition of the responses to specific stimulation steps (bottom left part). Here we chose to reduce the response amplitude dependent on the two steps before the current stimulation. In the second part of the movie, an additional component is seen starting at a shift of 47 steps in the cross-correlation result (second slice of the second-order kernel). (The full movie associated with this figure can be found in the Supplemental data section.)

plitude modulations as examples simply for educational reasons because it may be much easier (a) to compare amplitude changes between different waveforms than implicit time changes and (b) to follow the superposition of different waveforms with such a simplified scenario.

Second-order kernel, second slice

Similar results can be observed for the *second slice of the second-order kernel*, where the interval between the two observed points in time (blue rectangles) is two steps (Movie 6a in Figure 6). The cross-correlation shows that this interaction coincides with a shift of the m-sequence by 47 steps. In Movie 6b (Figure 6) a stimulus two steps before the current stimulus (white, black, and white rectangles in the bottom left part of Movie 6b) leads to a smaller modulation of the response than a stimulus that directly precedes the current stimulus (black, white, and white rectangles in the bottom left part of Movie 6b). When both preceding stimulations contain a stimulus (three white rectangles in the bottom left part of Movie 6b), the amplitude reduction is simply a summation of the amplitude reductions of both situations with only one preceding stimulus. The cross-correlation result shows two significant second-order kernel responses. Compared with Movie 5b, an additional second slice of the second order kernel response appears exactly 47 steps after the first-order response, as expected from Movie 6a.

Third- and higher order kernels

Finally, the *third-order kernel* indicates a processing that depends on three subsequent points in time (blue rectangles in Movie 7a of Figure 7). Again, this interaction turns out to occur with the same m-sequence as the original stimulation, in this case shifted by 97 steps. An additional third-order kernel response (bottom right part of Movie 7b of Figure 7) is seen with a delay of 97 steps after the first-order kernel in the cross-correlation result. Compared with Movie 6b, this third-order kernel is present because the response to three subsequent stimulations (here a flat waveform) cannot be derived by adding the effect of both individual preceding stimulations. Thus, all three steps are required to explain the response pattern in the bottom left part of Movie 7b.

It is obvious that the existence of such higher order kernels must be considered early enough when a specific experiment is designed. If the retinal or cortical processing of visual stimulation shows adaptational effects and if the preceding two, three, or more steps have an impact on the processing of the current stimulation, then we expect significant responses at the corresponding shifts for the second-, third-, or even higher order kernels in the cross-correlation response. The existence of such higher order kernels reduces the number of independent stimulation fields even more. If another field would be stimulated by the same m-sequence with a delay that corresponds to the occurrence of the second- or third-order kernel (47, 87, or 97 steps in our example), then we would expect a cross-contamination between these

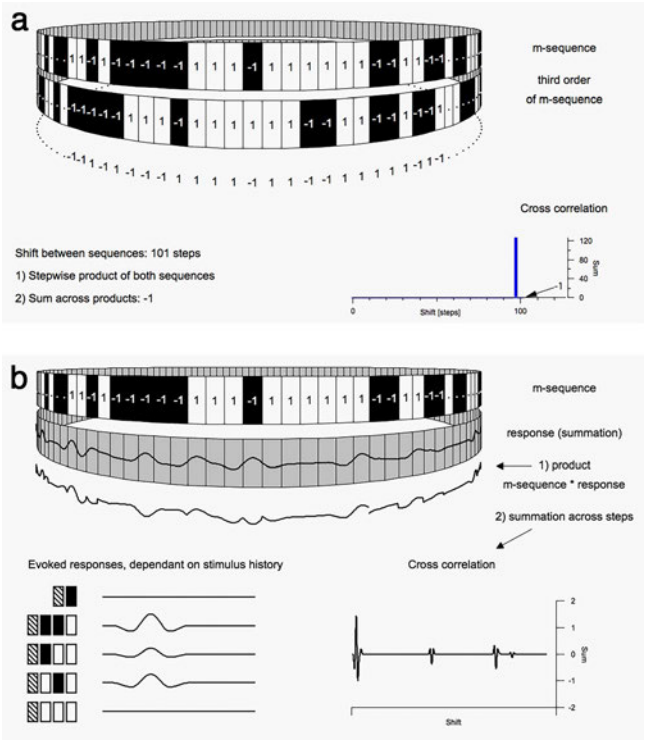

Figure 7. Third-order kernel. The movies demonstrate (a) the interaction in the processing of three subsequent stimulation steps and (b) the corresponding data analysis. (a) In order to evaluate an interaction of three subsequent steps of the m-sequence cycle, a product of three stimulation steps (highlighted in blue) is considered. The corresponding sequence is also a shifted version of the original m-sequence, here shifted by 97 steps. (b) Similar to Figure 6, the responses depend on three subsequent stimulation steps. In contrast to Figure 6, however, the response to a train of three stimulations (three white rectangles in the bottom left part) cannot be derived from the summation of the two stimulus sequences, where only one step contained a stimulus. As a consequence, the response pattern cannot be explained by second-order kernels alone. An additional third-order kernel response is seen in the cross-correlation result starting at a shift of 97 steps (third-order kernel). (The full movie associated with this figure can be found in the Supplemental data section.)

responses from different fields (Hagan, Fisher, & Brown, 2006; Ireland et al., 2002; Keating & Parks, 2006; Odom, 2006).

In summary, m-sequence recordings can be easily analyzed with a single cross-correlation procedure that yields the evoked first-order responses as well as all higher order kernel responses for all stimulation fields. The art of designing such m-sequence experiments is to ensure that all these possible responses can be extracted without any cross-contamination between all stimulation fields and between all significant kernel orders of all stimulation fields. How can we find such appropriate m-sequences?

Which m-sequence to use?

We have demonstrated the cross-correlation procedure and the existence of higher order kernel components for a simplified situation of only one stimulation field. Figure 8a summarizes the cross-correlation results of the original m-sequence (Figure 4) with those shifted m-sequences representing the three higher order kernels (Figures 5 through 7). In Figure 8a we also indicated the minimal delay of 10 steps between these possible components. This minimal delay is a critical factor when deciding on the choice of a specific m-sequence. For this one-field stimulation the response of the first slice of the second-order kernel should have a duration of less than 10 steps; otherwise it would overlap with the following third-order kernel response (cross-contamination) and it would be impossible to separate both components.

In general, the rationale is identical for a larger number of stimulation fields (e.g., for the seven fields in Movie 3 that were stimulated with the same, but shifted, m-sequence). The seven individual responses are found in the cross-correlation result with the same temporal shift. This follows directly from the description of the cross-correlation procedure. When the m-sequence stimulates two different fields with a time delay of 20 steps, their responses are delayed in the cross-correlation response by 20 steps, too. Thus, the cross-correlation is an appropriate and elegant tool for isolating the response of the different stimulation fields (Sutter, 2001; Sutter & Tran, 1992).

Under realistic conditions with about 60 different stimulation fields, the m-sequence with a length of 127 steps that we used throughout all examples would be much too short. This can be seen from Figure 8b, where we used a shift of 20 steps for the m-sequence of the second stimulation field. It can be seen that this shift of 20 steps applies not only to the first-order kernel but also to all other higher order kernels. It can be seen from Figure 8b that it would be impossible to stimulate a third field without reducing the minimum delay below 10 steps. The only solution would be a much longer m-sequence, which would allow the detection of all relevant higher order kernels for all stimulation fields without cross-contamination within the cross-correlation result.

If the m-sequence technique is to be applied to a new diagnostic or scientific question, we recommend the following procedure:

- Start with a full-field stimulation and a long m-sequence that allows one to study the higher order

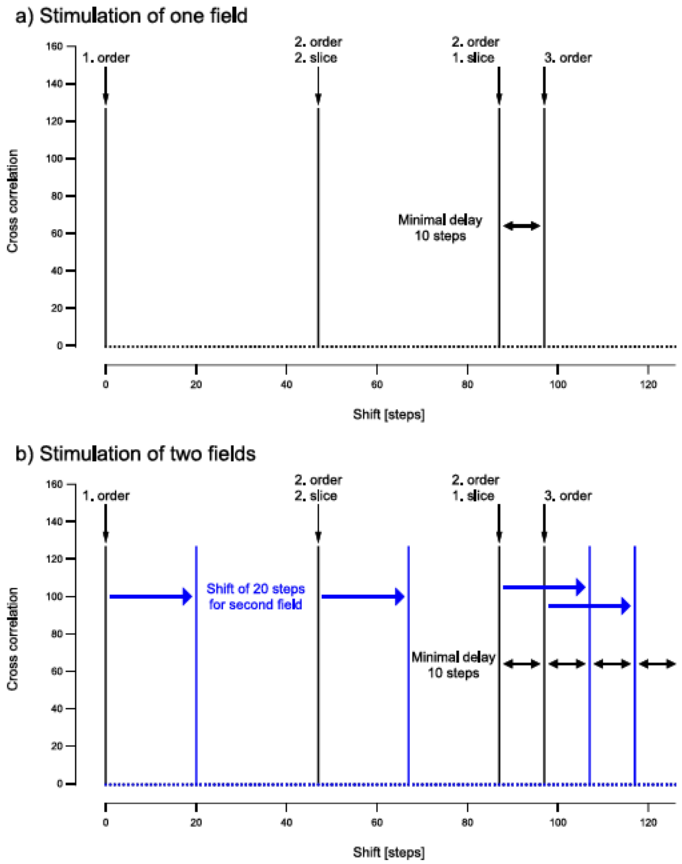

Figure 8. Strategic approach. The images demonstrate the strategic approach in designing m-sequence experiments for more than one stimulation field. (a) Summary of the cross-correlation results of Figures 4 through 7 for one stimulation field. To avoid overlapping of possible responses, the delay between kernels should exceed the expected duration of the respective evoked potentials. In this case the minimal delay between different kernels is 10 steps. Thus, the evoked response of all kernel orders must be back to the zero level within this time interval of 10 steps. Of course, the absolute time of this interval depends on the time for each step. (b) In multifocal settings the starting points within the same m-sequence for additional stimulation fields are shifted by a specific number of steps. The shift of the second field (here 20 steps) applies to all kernel orders (blue). In order to enable further stimulation fields and to preserve the minimum delay between all stimulation fields and all kernel orders, a much longer m-sequence is required.

kernels up to the fifth or sixth order. This allows one to (a) identify the number of relevant higher order kernels and (b) estimate the maximum duration of the evoked responses of these relevant kernels.

- Then an appropriate m-sequence can be chosen that has a minimum delay that is longer than the maximum response duration for all relevant higher order kernels and for all stimulation fields. In this way a cross-contamination between different stimulation fields and between different kernel orders is avoided.

Induced components

As demonstrated above, higher order kernels allow one to characterize the temporal interaction of subsequent responses and of the complexity and dynamics of the underlying neuronal processing. However, higher order kernels have an additional feature that is often overlooked and that is undesirable in most cases. Higher order kernel responses modify the waveforms of kernel responses with a lower order (Sutter, 2001). These modifications are denoted as *induced components* and can be demonstrated in Movies 5b, 6b, and 7b. For better visibility of these higher order kernels we combined the individual responses and the different kernel responses for Movies 4, 5b, 6b, and 7b in Figure 9.

Throughout all movies we assumed that a single stimulus without a preceding stimulus (first row in Figure 9a) would always lead to the same response. In Movie 4 this response was identical to the first-order kernel response (Figure 9, first column). Movies 5b, 6b, and 7b differed from Movie 4 in their amplitude reduction in response to different prestimulus histories. The first-order kernel response showed an average amplitude across all these prestimulus histories. However, the first-order responses also showed some response components after the initial major peaks that were not included in the original waveforms. These are the induced components and are marked with one or two asterisks in the first row of Figure 9b. The first slice of the second-order kernel shows a similar induced component (three asterisks in the second row of Figure 9b).

What is the origin of these induced components? In generating the recorded signal in Movies 5 through 7, we looked back into the prestimulus history at a specific step in the m-sequence. However, we could also look into the future of each of these steps. As the cross-correlation between m-sequence and recorded waveform calculates an average across all stimulus configurations, the corresponding part of the cross-correlation response is a mixture of situations where a future stimulus is preceded by another stimulus or by no stimulus. Thus, the same arguments that explain the existence of higher order kernels predict that lower order kernels (e.g., the first-order kernel) should show some intrusion from these higher order kernels with a specific time delay (Sutter, 2001).

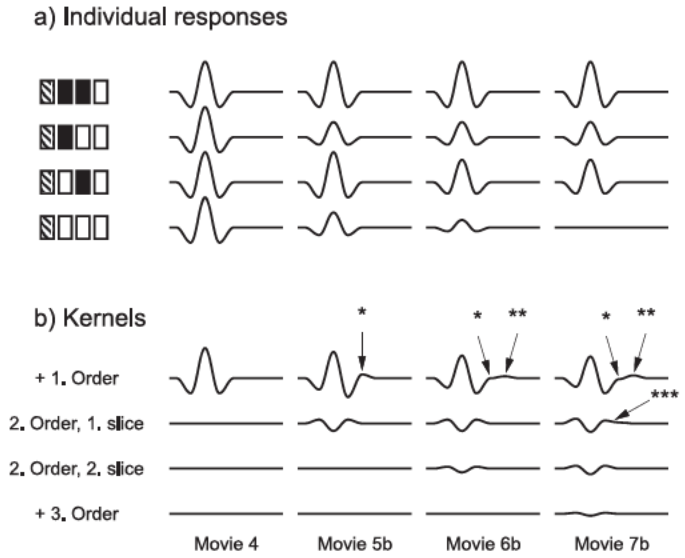

Figure 9. Induced components. Temporal interaction of subsequent responses and the complexity and dynamics of the underlying neuronal processing leads to modification of the waveforms of kernel responses with a lower order by higher order kernels (induced components). The columns show the results of Movies 4 through 7. (a) The top shows the respective options of evoked potentials dependent on the current and previous steps. (b) The bottom half illustrates the appropriate waveforms of the kernel responses. When a stimulation sequence evokes a significant first slice of the second-order kernel response (second to last column, referring to Figures 5 through 7), the first-order kernel shows an induced component after the initial major peak (first column, referring to Figure 4), highlighted by one asterisk. Additional induced components from the second slice of the second-order kernel (two asterisks) and of the third-order kernel (three asterisks) can be found in kernel waveforms with a lower order.

Synthesis

The last section on induced components may lead to certain confusion for the beginner in the field of m-sequence based electrophysiology. Some simple rules of thumb (e.g., that the first-order kernel shows the averaged response across all stimulus situations) may be correct, but they may turn out to be more complex than expected. Even a first-order kernel is modulated by temporal interactions as indicated by induced components. If we have recorded and analyzed the different kernel orders, we might want to predict the responses to different individual prestimulus histories as indicated in the lower left parts of Movies 4, 5b, 6b, and 7b.

Is there a way to eliminate the induced components? The answer to this question is *yes*. If we have available all relevant higher order kernels, we can predict the response of the visual system to any arbitrary sequence of stimulation (Sutter, 2000, 2001). This is illustrated in Movie 10a (Figure 10). Here we use the response pattern as shown in Movie 7b with significant responses up to the third-order kernel. In the top part of Movie 10a we synthesize a response to some arbitrary single, double, or triple stimulations in the same way as before. Responses to specific prestimulus conditions are superimposed and lead to the recorded waveform in the top yellow rectangle.

How can we synthesize the same waveform from the different kernel orders? This process is demonstrated in the bottom part of Movie 10a. First, the four kernels are assigned a binary number with three digits. Each **1** in this number indicates whether a specific point in time is relevant for the corresponding kernel. The prestimulus history for each order is always described by the first two digits, where the third digit is always **1** and describes the current stimulus. In the following we superimpose these kernel responses either with a positive sign when the three digits contain an odd number of **1**s (first order, third order) or with a negative sign when the three digits contain an even number of **1**s (first and second slice of the second-order kernel). Whether these kernel responses are superimposed at all is determined by a bitwise logical AND operation between the m-sequence stimulus history and all kernel order binary numbers. Only when the result has an odd number of **1**s (which coincides with an odd parity) the corresponding kernel order is superimposed (lower yellow rectangle).

Movie 10b (Figure 10) shows another example with a faster stimulation frequency. Again, the synthesis by higher order kernels (bottom yellow rectangle) leads to the same waveform as the synthesis by individual responses (top yellow rectangle). The procedure for deriving the waveform by kernel orders is much more complicated than the superposition of individual responses. The major advantage, however, is that it can be applied to every m-sequence recording. While it is usually impossible to superimpose individual waveforms because they are unknown in real-world situations, the kernel responses follow directly from the cross-correlation analysis and are always available.

In the presented examples, we made specific assumptions about these individual responses in order to see what the consequences of these assumptions would be for the different kernel orders. The kernel-based procedure (lower yellow rectangles in Movie 10a, b) is also an excellent way to get rid of the induced components. For example, if one would like to know the response of the visual system to a single stimulus, the first part of Movie 10a is a recipe. Even in the simple case of a single stimulus, all relevant kernel order responses have to be added at some point in time to yield the correct response. In this way all individual responses (top left part of Movie 10a, b) can be derived

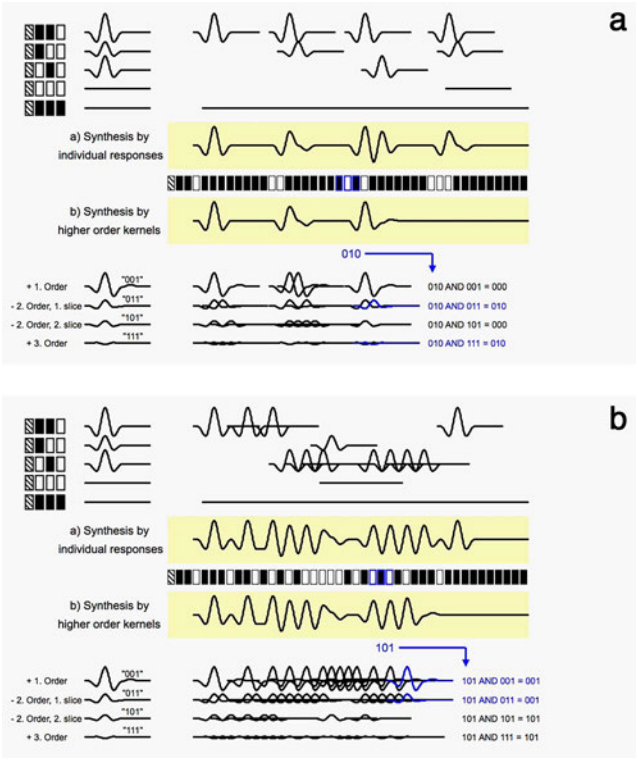

Figure 10. Synthesis. Results of relevant kernels enable one to predict the response of the visual system to an arbitrary sequence of stimulation, here demonstrated for a (a) slow and (b) fast stimulation frequency. The top part of both movies shows the individual evoked responses to some arbitrary stimulation equivalent to Movie 7b. Progressing the stimulation sequence in the middle (respective step is highlighted in blue), individual evoked responses are superimposed and lead to the response summation in the top yellow rectangle. In the bottom part of both movies the synthesis of the same waveform by the different kernel order responses is demonstrated. An identical waveform (bottom yellow rectangle) can be generated by superimposing relevant kernel order responses. Whether a specific kernel order is added at a specific point in time depends on a bitwise AND operation between the stimulation sequence (black and white rectangles between the two yellow rectangles) and a binary signature of each kernel order. The AND operation is calculated for a specific number of relevant steps representing the prestimulus history (here three; highlighted in blue). Whether a specific kernel order is added or subtracted depends on the parity of the kernel signature. The option to derive the response of the visual system to any arbitrary stimulation sequence is a major advantage of m-sequence stimulation because it allows one to synthesize experimental data to many different stimulation sequences from a single recording. (The full movie associated with this figure can be found in the Supplemental data section.)

from the collection of higher order kernels (Sutter, 2000, 2001).

Clinical application

Multifocal electrophysiology based on m-sequences has been used in different diseases as a clinical diagnostic tool (Betsuin et al., 2001; Hood et al., 2000, 2004; Hood & Zhang, 2000; Lai et al., 2007). Apart from settings determined in the standards and guidelines (Hood et al., 2012; Marmor et al., 2003), other human factors such as age and refractive errors influence the evoked potentials and therefore necessitate standard values (Fortune, Zhang, Hood, Demirel, & Johnson, 2004; Pieh, Hoffmann, & Bach, 2005). As a functional testing, multifocal electrophysiology also requires long measurement periods compared with imaging techniques. However, the unique objectivity of this functional testing has led to the wide spectrum of application areas. Several review articles have been published on the aspect of clinical application of m-sequence based multifocal technique, and readers can refer to these publications for further information (Betsuin et al., 2001; Hood, 2006; Hood & Greenstein, 2003; Hood et al., 2003; Hood, Odel, Chen, & Winn, 2003; Hood & Zhang, 2000; Lai et al., 2007; Palmowski, 2003). The following paragraphs describe how these applications have been using the m-sequence based multifocal electrophysiology.

mfERG is usually executed in a flash stimulation setting. As discussed in M-sequence based stimulation, **1**s represent the flash and **1**s typify pauses. The main response can be found in the first-order kernel using these settings. Higher order kernels usually have much smaller amplitudes than the first-order flash kernel (Figures 4 through 7). Even if higher order kernels contain additional information and induce components to lower order kernels, most of the time only the first-order kernel has been evaluated to examine the extent of impairment of retinal diseases. However, the simple evaluation has been sufficient to show that changes in mfERG correlate with morphologic changes. For example, in patients with age-related macular degeneration, central serous chorioretinopathy or retinal vascular occlusion mfERG reveals reduced amplitudes in respective affected areas (Feigl, Brown, Lovie-Kitchin, & Swann, 2004, 2006; Gerth, 2009; Gin, Luu, & Guymer, 2011; Hvarfner, Andreasson, & Larsson, 2006; Lai, Chan, & Lam, 2004; Lai et al., 2008; Vajaranant, Szlyk, Fishman, Gieser, & Seiple, 2002; Wildberger & Junghardt, 2002; Wu, Ayton, Guymer, & Luu, 2014; Wu, Ayton, Makeyeva, Guymer, & Luu, 2015; Yavas, Küsbeci, & Inan, 2014; Yip et al., 2010). Consequently, the

multifocal techniques help distinguish hereditary or other rare disease. This might allow the investigator to focus adjacent genetic testing, implying a great sociopolitical advantage (Kellner et al., 2015). The sole evaluation of the first-order kernel of the mfERG already enables one to measure potential retinal impairment by toxic agents such as chloroquine or traumas (Adam, Covert, Stepien, & Han, 2012; Browning, 2013; Gjoerloff, Andreasson, & Ghosh, 2006; Kellner, Weinitz, & Kellner, 2009; Loevestam-Adrian, Andreasson, & Ponjavic, 2004; Marmor et al., 2011; Nebbioso, Grenga, & Karavitis, 2009; Park et al., 2011; Penrose et al., 2003; Stangos et al., 2007; Verdon, 2008). This potential allows perioperative monitoring in retinal surgery. In expert opinions, mfERG can be used to objectify the extent of impairment (Andreasson & Ghosh, 2014; Moschos et al., 2001; Shimada et al., 2011; Wallenten, Andreasson, & Ghosh, 2008).

Evaluation of higher order kernels and other approaches such as oscillatory potentials or slow double-stimulation mfERG have been used to examine the level of impairment in retinal diseases (e.g., mfERG results suggest that the inner retina is first affected in diabetic retinopathy). Alterations in mfERG might even be measurable in diabetic patients before structural changes of diabetic retinopathy occur, suggesting an opportunity to predict the disease progression (Bearse et al., 2006; Bearse & Ozawa, 2014; Chan et al., 2011; Han et al., 2004; Harrison et al., 2011; Kim, Song, & Yu, 2007; Laron et al., 2012; Ng, Bearse, Schneck, Barez, & Adams, 2008; Onozu & Yamamoto, 2003; Xu, Hu, Huang, Huang, & Chen, 2006; Zhu, Zhang, Wang, & Xu, 2014).

Due to the assignment of **1**s and **1**s in pattern stimulation, the main response is found in the first slice of the second-order kernel because this kernel characterizes the inversion (see M-sequence based stimulation). Therefore, the evaluation of pattern stimulation based electrophysiology focuses on the respective kernel. As the Pattern ERG might be more sensitive than the Flash ERG regarding function impairment and progression, the combination has been shown to roughly appraise future progress in some diseases. Hence, monofocal Pattern ERG was already used for classifications like in Stargardt macular dystrophy (Fujinami et al., 2013; Lois, Holder, Bunce, Fitzke, & Bird, 2001).

The Pattern ERG is thought to derive from ganglion cells (Celesia, 1988; Harrison, Viswanathan, & Malinovsky, 2006). In combination with the topographic map of retinal functions enabled by the multifocal setting, multifocal Pattern ERG suggests a benefit in the assessment of glaucoma patients (Harrison et al., 2006; Stiefelmeyer, Neubauer, Berninger, Arden, & Rudolph, 2004). Reduced amplitudes are associated with visual field defects as well as nerve fiber layer thickness and can even be found before manifest glaucoma occurs (Bach, 2001; Bach & Hoffmann, 2008; Bach & Poloschek, 2013; Bach et al., 2006; Rao, Singh, Mukherjee, & Chowdhury, 2015). Various modifications of the mfERG stimulation such as fast flicker, low contrast, slow sequence, global flash, two flash, and luminance modulation have been developed in recent years in order to improve validity and effectiveness in the diagnosis of glaucoma (Chan, 2005; Chan, Ng, & Chu, 2011; Chu, Chan, & Brown, 2006, 2007; Chu et al., 2012; Kramer et al., 2013; Ledolter, Kramer, Todorova, Schötzau, & Palmowski-Wolfe, 2013; Ledolter, Monhart, Schoetzau, Todorova, & Palmowski-Wolfe, 2015; Palmowski-Wolfe, Allgayer, Vernaleken, Schötzau, & Ruprecht, 2006; Palmowski-Wolfe, Todorova, Orguel, Flammer, & Brigell, 2007).

Even if mfVEP can be used in a flash stimulation setting, it is usually executed with pattern stimulation. Evaluating the first slice of the second-order kernel, scotomas are associated with reductions of amplitude of the recorded potentials in the corresponding field. Pattern mfVEP therefore allows topographic mapping of retinal function of the central 20° to 50° (Hood & Greenstein, 2003; Lai et al., 2007), which also enables one to measure visual field defects caused by glaucoma (Bach & Poloschek, 2013; Graham, Klistorner, Grigg, & Billson, 2000; Klistorner & Graham, 2000; Klistorner, Graham, & Martins, 2000) as well as optic neuropathy, papillorenal syndrome, or other diseases of the visual system (Chen, Odel, Miller, & Hood, 2002; Hood et al., 2000; Wolff, Bearse, Schneck, Barez, & Adams, 2010). Using mfVEP, amplitudes and latencies differentiate neuronal degeneration and demyelinization, respectively. Consequently, mfVEP is highly sensitive in diseases such as multiple sclerosis or secondary compression due to craniocerebral injury, bleeding, and cerebral neoplasia enabling an early objective recognition (Jayaraman et al., 2010; Laron et al., 2010).

Consideration of both mfERG and mfVEP kernels can help localize the site of dysfunction in the visual system. Alterations within the retina can be differentiated from impairment of the optic nerve and further central parts because mfERGs are normal in isolated optic nerve disease (Hoffman et al., 2003; Hood et al., 2000; Zhang, 2003).

In previous sections we did not focus on other fine strategies such as the Laplacian method, or the combination of signals from different derivations and kernels. Particularly using these strategies, scotomas can be revealed more sensitively with multifocal electrophysiology suggesting identifying defects even before they are visible in conventional perimetry (Goldberg, Graham, & Klistorner, 2002; Hood & Zhang, 2000; Hood, Zhang, Hong, & Chen, 2002;

Klistorner et al., 2007; Meigen & Krämer, 2007). Interocular comparison is a promising strategy for detecting scotomas and takes advantage of the fact that corresponding locations in the retina of both eyes are represented at similar locations in the visual cortex. However, it is limited to the detection of monocular visual field defects (Graham et al., 2000; Hood et al., 2000).

A new application of m-sequence based multifocal technique can be seen in the evaluation of rare structural alterations in the visual system, such as in patients with ocular albinism. Here, a deficient embryonic formation of the optic chiasm is frequently associated, as has been shown by the combination of full-field or Pattern VEP and functional magnetic resonance tomography (Apkarian, 1994; Apkarian, Reits, & Spekreijse, 1984; Bouzas, Caruso, Drews-Bankiewicz, & Kaiser-Kupfer, 1994; Hoffmann, Lorenz, Morland, & Schmidtborn, 2005; Hoffmann, Tolhurst, Moore, & Morland, 2003; Morland, Hoffmann, Neveu, & Holder, 2002; Pott, Jansonius, & Kooijman, 2003). Measurement of various small locations in the visual field using the mfVEP enables one to get more useful information in the future.

It has been shown that amplitudes in full-field or Pattern VEP correlate with visual acuity (Groneberg & Teping, 1981; Teping, 1981). However, VEP-based estimates of visual acuity might be inaccurate despite several improvements (Bach, Maurer, & Wolf, 2008; Kurtenbach, Langrová, Messias, Zrenner, & Jägle, 2013; Regan & Spekreijse, 1986). Hence, multifocal techniques record summed potentials of small regions of the central visual field suggesting more precise calculation of central visual function (Jiang et al., 2011). This suggests a great benefit in the investigation of visual processing in nonverbal subjects such as small children or animals (Crewther, Luu, Kiely, Kowal, & Crewther, 2004).

Another upcoming field of application is evaluation after retinal implants, gene therapy, and cell therapy. mfERG and mfVEP provide the opportunity to assess the efficacy objectively (Christiansen et al., 2012; Li, Yin, Chen, Chen, & Liu, 2009).

Finally, adaptation and settings in multifocal electrophysiology such as colored stimulation allow one to differentiate cell types, enabling the separate investigation of the topographic function of the rod- and the cone-system, or to distinguish cone types in the examination of color blindness (Feigl et al., 2004, 2006; Holopigian, Seiple, Greenstein, Hood, & Carr, 2002; Holopigian et al., 2005; Hood, Wladis, Shady, Holopigian, & Seiple, 1998). By evaluation of different higher order kernels, additional information can be obtained concerning retinal and cortical processing of visual stimulation. The synthesis function (see Synthesis) has not yet been used in daily clinical routine, mainly because it appears to be a complex procedure, although it offers a great advantage in the prediction and calculation of specific responses. With this review we hope to clarify the opportunities of m-sequences in order to motivate scientists to use m-sequences in their future research with all of the promising features, including the synthesis function.

Keywords: electroretinogram, multifocal electroretinogram, visual evoked potential, multifocal visual evoked potential, m-sequence, kernels, cross-correlation, synthesis function

Acknowledgments

The authors thank Bob Wilberscheid for critical comments on the article. This work was supported by the Bundesministerium für Bildung und Forschung (IZKF Würzburg, Grant 01KS9603). The sponsor or funding organization had no role in the design or conduct of this research.

Commercial relationships: none.
Corresponding author: Thomas Meigen.
Email: info@meigensmartsolutions.de.
Address: Dr. Thomas Meigen Smart Solutions, Würzburg, Germany.

References

Adam, M., Covert, D., Stepien, K., & Han, D. (2012). Quantitative assessment of the 103-hexagon multifocal electroretinogram in detection of hydroxychloroquine retinal toxicity. *British Journal of Ophthalmology, 96*(5), 723 729.

Andreasson, S., & Ghosh, F. (2014). Cone implicit time as a predictor of visual outcome in macular hole surgery. *Graefe's Archives of Clinical and Experimental Ophthalmology, 252*(12), 1903 1909.

Apkarian, P. (1994). VEP in albinism. *Ophthalmology, 101,* 1867 1868.

Apkarian, P., Reits, D., & Spekreijse, H. (1984). Component specificity in albino VEP asymmetry: Maturation of the visual pathway anomaly. *Experimental Brain Research, 53,* 285 294.

Bach, M. (2001). Electrophysiological approaches for early detection of glaucoma. *European Journal of Ophthalmology, 11,* 41 49.

Bach, M., & Hoffmann, M. (2008). Update on the

pattern electroretinogram in glaucoma. *Optometry and Vision Science, 85*(6), 385 395.

Bach, M., Maurer, J. P., & Wolf, M. E. (2008). Visual evoked potential-based acuity assessment in normal vision, artificially degraded vision, and in patients. *British Journal of Ophthalmology, 92,* 396 403.

Bach, M., & Poloschek, C. (2013). Electrophysiology and glaucoma: Current status and future challenges. *Cell and Tissue Research, 253*(2), 287 296.

Bach, M., Unsoeld, A., Philippin, H., Staubach, F., Maier, P., Walter, H., . . . Funk, J. (2006). Pattern ERG as an early glaucoma indicator in ocular hypertension: A long-term, prospective study. *Investigative Ophthalmology & Visual Science, 47*(11), 4881 4887. [PubMed] [Article]

Balachandran, C., Klistorner, A. I., & Graham, S. L. (2003). Effect of stimulus check size on multifocal visual evoked potentials. *Documenta Ophthalmologica, 106,* 183 188.

Baseler, H. A., Sutter, E. E., Klein, S. A., & Carney, T. (1994). The topography of visual evoked response properties across the visual field. *Electroencephalography and Clinical Neurophysiology, 90*(1), 65 81.

Bearse, M., Adams, A., Han, Y., Schneck, M., Ng, J., Bronson-Castain, K., & Barez, S. (2006). A multifocal electroretinogram model predicting the development of diabetic retinopathy. *Progress in Retinal and Eye Research, 25*(5), 425 448.

Bearse, M., & Ozawa, G. (2014). Multifocal electroretinography in diabetic retinopathy and diabetic macular edema. *Current Diabetes Reports, 14*(9), 526.

Betsuin, Y., Mashima, Y., Ohde, H., Inoue, R., & Oguchi, Y. (2001). Clinical application of the multifocal VEPs. *Current Eye Research, 22*(1), 54 63.

Bouzas, E. A., Caruso, R. C., Drews-Bankiewicz, M. A., & Kaiser-Kupfer, M. I. (1994). Evoked potential analysis of visual pathways in human albinism. *Ophthalmology, 101,* 309 314.

Browning, D. (2013). Impact of the revised American Academy of Ophthalmology guidelines regarding hydroxychloroquine screening on actual practice. *American Journal of Ophthalmology, 155*(3), 418 428.

Celesia, G. (1988). Anatomy and physiology of visual evoked potentials and electroretinograms. *Neurologic Clinics, 6*(4), 657 679.

Chan, H. (2005). Detection of glaucomatous damage using multifocal ERG. *Clinical and Experimental Optometry, 88*(6), 410 414.

Chan, H., Chu, P., Lung, J., Ho, W., Ting, P., Sum, R., & Ng, Y. (2011). Detection of early functional changes in diabetic retina using slow double-stimulation mfERG paradigm. *British Journal of Ophthalmology, 95*(11), 1560 1563.

Chan, H., Ng, Y., & Chu, P. (2011). Applications of the multifocal electroretinogram in the detection of glaucoma. *Clinical and Experimental Optometry, 94*(3), 247 258.

Chen, C. S., Odel, J. G., Miller, J. S., & Hood, D. C. (2002). Multifocal visual evoked potentials and multifocal electroretinograms in papillorenal syndrome. *Archives of Ophthalmology, 120,* 870 871.

Christiansen, A., Kiilgaard, J., Smith, M., Ejstrup, R., Wnek, G., Prause, J., . . . La Cour, M. (2012). The influence of brightness on functional assessment by mfERG: A study on scaffolds used in retinal cell transplantation in pigs. *Stem Cells International, 2012,* 263 264.

Chu, P., Chan, H., & Brown, B. (2006). Glaucoma detection is facilitated by luminance modulation of the global flash multifocal electroretinogram. *Investigative Ophthalmology & Visual Science, 47*(3), 929 937. [PubMed] [Article]

Chu, P., Chan, H., & Brown, B. (2007). Luminance-modulated adaptation of global flash mfERG: Fellow eye losses in asymmetric glaucoma. *Investigative Ophthalmology & Visual Science, 48*(6), 2626 2633. [PubMed] [Article]

Chu, P., Ng, Y., To, C., So, K., Brown, B., & Chan, H. (2012). Luminance-modulated adaptation in the global flash mfERG: A preliminary study of early retinal functional changes in high-risk glaucoma patients. *Graefe's Archives of Clinical and Experimental Ophthalmology, 250*(2), 261 270.

Citron, M., Emerson, R., & Wollmann, D. (1983). White noise analysis of cortical directional selectivity in cat. *Brain Research, 279,* 271 277.

Collins, A., & Sawhney, B. (1993). Pseudorandom binary sequence stimulation applied to the visual evoked response: Normative data and a comparative study with pattern and flash stimulation. *Documenta Ophthalmologica, 83*(2), 163 173.

Crewther, D., Luu, C., Kiely, P., Kowal, L., & Crewther, S. (2004). Clinical application of the multifocal visual evoked potential. *Clinical and Experimental Optometry, 87*(3), 163 170.

Davies, W. (1970). *System identification for self-adaptive control.* New York, NY: Wiley.

Feigl, B., Brown, B., Lovie-Kitchin, J., & Swann, P. (2004). Cone-mediated multifocal electroretinogram in early age-related maculopathy and its

relationships with subjective macular function tests. *Current Eye Research, 29,* 327 336.

Feigl, B., Brown, B., Lovie-Kitchin, J., & Swann, P. (2006). The rod-mediated multifocal electroretinogram in aging and in early age-related maculopathy. *Current Eye Research, 31,* 635 644.

Fortune, B., Zhang, X., Hood, D. C., Demirel, S., & Johnson, C. A. (2004). Normative ranges and specificity of the multifocal VEP. *Documenta Ophthalmologica, 109*(1), 87 100.

Fricker, S., & Sanders, J. (1975). A new method of cone electroretinography: The rapid random flash response. *Investigative Ophthalmology & Visual Science, 14*(2), 131 137. [PubMed] [Article]

Fujinami, K., Lois, N., Davidson, A., Mackay, D., Hogg, C., Stone, E., . . . Michaelides, M. (2013). A longitudinal study of Stargardt disease: Clinical and electrophysiologic assessment, progression, and genotype correlations. *American Journal of Ophthalmology, 155*(6), 1075 1088.

Gerth, C. (2009). The role of the ERG in the diagnosis and treatment of age-related macular degeneration. *Documenta Ophthalmologica, 118*(1), 63 68.

Gin, T., Luu, C., & Guymer, R. (2011). Central retinal function as measured by the multifocal electroretinogram and flicker perimetry in early age-related macular degeneration. *Investigative Ophthalmology & Visual Science, 52,* 9267 9274. [PubMed] [Article]

Gjoerloff, K., Andreasson, S., & Ghosh, F. (2006). mfERG in normal and lesioned rabbit retina. *Graefe's Archives of Clinical and Experimental Ophthalmology, 244*(1), 83 89.

Goldberg, I., Graham, S. L., & Klistorner, A. I. (2002). Multifocal objective perimetry in the detection of glaucomatous field loss. *American Journal of Ophthalmology, 133,* 29 39.

Golomb, S. W. (1982). *Shift register sequences*. Laguna Hills, CA: Aegean Park Press.

Graham, S. L., Klistorner, A. I., Grigg, J. R., & Billson, F. A. (2000). Objective VEP perimetry in glaucoma: Asymmetry analysis to identify early deficits. *Journal of Glaucoma, 9,* 10 19.

Groneberg, A., & Teping, C. (1981). Visually evoked cortical potentials (VECP) in patients with doubtful impairment of central vision. *Klinische Monatsblätter für Augenheilkunde, 179,* 173 176.

Hagan, R., Fisher, A., & Brown, M. (2006). Examination of short binary sequences for mfERG recording. *Documenta Ophthalmologica, 113,* 21 27.

Han, Y., Bearse, M., Schneck, M., Barez, S., Jacobsen, C., & Adams, A. (2004). Multifocal electroretinogram delays predict sites of subsequent diabetic retinopathy. *Investigative Ophthalmology & Visual Science, 45*(3), 948 954. [PubMed] [Article]

Harrison, W., Bearse, M., Ng, J., Jewell, N., Barez, S., Burger, D., . . . Adams, A. (2011). Multifocal electroretinograms predict onset of diabetic retinopathy in adult patients with diabetes. *Investigative Ophthalmology & Visual Science, 52*(2), 772 777. [PubMed] [Article]

Harrison, W., Viswanathan, S., & Malinovsky, V. (2006). Multifocal pattern electroretinogram: Cellular origins and clinical implications. *Optometry and Vision Science, 83*(7), 473 485.

Heinemann-Vernaleken, B., Palmowski, A., Allgayer, R., & Ruprecht, K. (2001). Comparison of different high resolution multifocal electroretinogram recordings in patients with age-related maculopathy. *Graefe's Archives of Clinical and Experimental Ophthalmology, 239*(8), 556 561.

Hoffmann, M. B., Lorenz, B., Morland, A. B., & Schmidtborn, L. (2005). Misrouting of the optic nerves in albinism: Estimation of the extent with visual evoked potentials. *Investigative Ophthalmology & Visual Science, 46,* 3892 3898. [PubMed] [Article]

Hoffmann, M. B., Straube, S., & Bach, M. (2003). Pattern-onset stimulation boosts central multifocal VEP responses. *Journal of Vision, 3*(6):4, 432 439, doi:10.1167/3.6.4. [PubMed] [Article]

Hoffmann, M. B., Tolhurst, D., Moore, A., & Morland, A. B. (2003). Organization of the visual cortex in human albinism. *The Journal of Neuroscience, 23,* 8921 8930.

Holopigian, K., Seiple, W., Greenstein, V., Hood, D., & Carr, R. (2002). Local cone and rod system function in progressive cone dystrophy. *Investigative Ophthalmology & Visual Science, 43*(7), 2364 2373. [PubMed] [Article]

Holopigian, K., Shuwairi, S., Greenstein, V., Winn, B., Zhang, X., Carr, R., & Hood, D. (2005). Multifocal visual evoked potentials to cone specific stimuli in patients with retinitis pigmentosa. *Vision Research, 45*(25 26), 3244 3252.

Hood, D. (2006). The multifocal electroretinographic and visual evoked potential techniques. In J. Heckenlively & G. Arden (Eds.), *Principles and practice of clinical electrophysiology of vision* (2nd ed., pp. 197 205). Cambridge, MA: MIT Press.

Hood, D., Bach, M., Brigell, M., Keating, D., Kondo, M., Lyons, J., . . . Palmowski-Wolfe, A. (2012). ISCEV standard for clinical multifocal electroretinography (2011 edition). *Documenta Ophthalmologica, 124,* 1 13.

Hood, D., Odel, J., Chen, C., & Winn, B. (2003). The multifocal electroretinogram. *Journal of Neuro-Ophthalmology, 23*(3), 225 235.

Hood, D., Odel, J., & Winn, B. (2003a). The multifocal visual evoked potential. *Journal of Neuro-Ophthalmology, 23*(4), 279 289.

Hood, D., Wladis, E., Shady, S., Holopigian, K., & Seiple, W. (1998). Rod multi-focal electroretinograms. *Investigative Ophthalmology & Visual Science, 39,* 1152 1162. [PubMed] [Article]

Hood, D. C., & Greenstein, V. C. (2003). Multifocal VEP and ganglion cell damage: Applications and limitations for the study of glaucoma. *Progress in Retinal and Eye Research, 22*(2), 201 251.

Hood, D. C., & Zhang, X. (2000). Multifocal ERG and VEP responses and visual fields: Comparing disease-related changes. *Documenta Ophthalmologica, 100,* 115 137.

Hood, D. C., Zhang, X., Greenstein, V. C., Kangovi, S., Odel, J. G., Liebmann, J. M., & Ritch, R. (2000). An interocular comparison of the multifocal VEP: A possible technique for detecting local damage to the optic nerve. *Investigative Ophthalmology & Visual Science, 41,* 1580 1587. [PubMed] [Article]

Hood, D. C., Zhang, X., Hong, J. E., & Chen, C. S. (2002). Quantifying the benefits of additional channels of multifocal VEP recording. *Documenta Ophthalmologica, 104*(3), 303 320.

Hood, D. C., Zhang, X., Rodarte, C., Yang, E. B., Ohri, N., Fortune, B., & Johnson, C. A. (2004). Determining abnormal interocular latencies of multifocal visual evoked potentials. *Documenta Ophthalmologica, 109*(2), 177 187.

Horton, J. C., & Hoyt, W. F. (1991). The representation of the visual field in human striate cortex. A revision of the classic Holmes map. *Archives of Ophthalmology, 109,* 816 824.

Hvarfner, C., Andreasson, S., & Larsson, J. (2006). Multifocal electroretinography and fluorescein angiography in retinal vein occlusion. *Retina, 26*(3), 292 296.

Ireland, J., Keating, D., Hoggar, S., & Parks, S. (2002). Identification of appropriate primitive polynomials to avoid cross-contamination in multifocal electroretinogram responses. *Medical & Biological Engineering & Computing, 40,* 471 478.

Jayaraman, M., Ambika, S., Gandhi, R. A., Bassi, S. R., Ravi, P., & Sen, P. (2010). Multifocal visual evoked potential recordings in compressive optic neuropathy secondary to pituitary adenoma. *Documenta Ophthalmologica, 121,* 197 204.

Jiang, L., Zhang, H., Xie, L., Jiao, X., Zhou, L., Ji, H., . . . Wang, N. (2011). Application of multifocal visual evoked potentials in the assessment of visual dysfunction in macular diseases. *Eye, 25*(10), 1302 1309.

Kalpadakis, P., & Rudolph, G. (2003). Multifocal ERG with the scanning laser ophthalmoscope: Query on the ideal configuration for attaining high resolution and result stability. *Graefe's Archives of Clinical and Experimental Ophthalmology, 241*(6), 522.

Keating, D., & Parks, S. (2006). Multifocal technique. In J. Heckenlively & G. Arden (Eds.), *Principles and practice of clinical electrophysiology of vision* (2nd ed., pp. 319 340). Cambridge, MA: MIT Press.

Kellner, S., Weinitz, S., & Kellner, U. (2009). Spectral domain optical coherence tomography detects early stages of chloroquine retinopathy similar to multifocal electroretinography, fundus autofluorescence and near-infrared autofluorescence. *British Journal of Ophthalmology, 93,* 1444 1447.

Kellner, U., Kellner, S., Weinitz, S., Farmand, G., Weber, B., & Stöhr, H. (2015). Inherited retinal or optic nerve disorders Five steps to diagnosis. *Klinische Monatsblätter für Augenheilkunde, 232,* 250 258.

Kim, S., Song, S., & Yu, H. (2007). Multifocal electroretinogram responses of the clinically normal retinal areas in diabetes. *Ophthalmic Research, 39*(5), 282 288.

Klein, S. (1992). Optimizing the estimation of nonlinear kernels. In R. Pinter & E. Nabat (Eds.), *Nonlinear vision* (pp. 109 170). Boca Raton, FL: CRC Press.

Klistorner, A., & Graham, S. L. (2000). Objective perimetry in glaucoma. *Ophthalmology, 107,* 2283 2299.

Klistorner, A., Graham, S. L., Martins, A., Grigg, J. R., Arvind, H., Kumar, R. S., . . . Billson, F. A. (2007). Multifocal blue-on-yellow visual evoked potentials in early glaucoma. *Ophthalmology, 114*(9), 1613 1621.

Klistorner, A. I., Graham, S. L., & Martins, A. (2000). Multifocal pattern electroretinogram does not demonstrate localised field defects in glaucoma. *Documenta Ophthalmologica, 100,* 155 165.

Kramer, S., Ledolter, A., Todorova, M., Schötzau, A., Orgül, S., & Palmowski-Wolfe, A. (2013). The 2-global flash mfERG in glaucoma: Attempting to increase sensitivity by reducing the focal flash luminance and changing filter settings. *Documenta Ophthalmologica, 126*(1), 57 67.

Kretschmann, U., Bock, M., Gockeln, R., & Zrenner,

E. (2000). Clinical applications of multifocal electroretinography. *Documenta Ophthalmologica, 100,* 99 113.

Kruth, D. (1981). *Semi-numerical algorithms* (2nd ed.). Reading, MA: Addison-Wesley.

Kurtenbach, A., Langrová, H., Messias, A., Zrenner, E., & Jägle, H. (2013). A comparison of the performance of three visual evoked potential-based methods to estimate visual acuity. *Documenta Ophthalmologica, 126*(1), 45 56.

Lai, T., Chan, W., & Lam, D. (2004). Transient reduction in retinal function revealed by multifocal electroretinogram after photodynamic therapy. *American Journal of Ophthalmology, 137*(5), 826 833.

Lai, T., Lai, R., Ngai, J., Chan, W., Li, H., & Lam, D. (2008). First and second-order kernel multifocal electroretinography abnormalities in acute central serous chorioretinopathy. *Documenta Ophthalmologica, 116*(1), 29 40.

Lai, T. Y., Chan, W. M., Lai, R. Y., Ngai, J. W., Li, H., & Lam, D. S. (2007). The clinical applications of multifocal electroretinography: A systematic review. *Survey of Ophthalmology, 52,* 61 96.

Larkin, R., Klein, S., Ogden, T., & Fender, D. (1979). Nonlinear kernel of the human ERG. *Biological Cybernetics, 35*(3), 145 160.

Laron, M., Bearse, M., Bronson-Castain, K., Jonasdottir, S., King-Hooper, B., Barez, S., . . . Adams, A. (2012). Interocular symmetry of abnormal multifocal electroretinograms in adolescents with diabetes and no retinopathy. *Investigative Ophthalmology & Visual Science, 53,* 316 321. [PubMed] [Article]

Laron, M., Cheng, H., Zhang, B., Schiffman, J. S., Tang, R. A., & Frishman, L. J. (2010). Comparison of multifocal visual evoked potential, standard automated perimetry and optical coherence tomography in assessing visual pathway in multiple sclerosis patients. *Multiple Sclerosis Journal, 16,* 412 426.

Ledolter, A., Kramer, S., Todorova, M., Schötzau, A., & Palmowski-Wolfe, A. (2013). The effect of filtering on the two-global-flash mfERG: Identifying the optimal range of frequency for detecting glaucomatous retinal dysfunction. *Documenta Ophthalmologica, 126*(2), 117 123.

Ledolter, A., Monhart, M., Schoetzau, A., Todorova, M., & Palmowski-Wolfe, A. (2015). Structural and functional changes in glaucoma: Comparing the two-flash multifocal electroretinogram to optical coherence tomography and visual fields. *Documenta Ophthalmologica, 130*(3), 197 209.

Li, S., Yin, Z., Chen, S., Chen, L., & Liu, Y. (2009). Rescue from light-induced retinal degeneration by human fetal retinal transplantation in minipigs. *Current Eye Research, 34*(7), 523 535.

Loevestam-Adrian, M., Andreasson, S., & Ponjavic, V. (2004). Macular function assessed with mfERG before and after panretinal photocoagulation in patients with proliferative diabetic retinopathy. *Documenta Ophthalmologica, 109*(2), 115 121.

Lois, N., Holder, G., Bunce, C., Fitzke, F., & Bird, A. (2001). Phenotypic subtypes of Stargardt macular dystrophy-fundus flavimaculatus. *Archives of Ophthalmology, 119*(3), 359 369.

MacWilliams, F., & Sloane, N. (1977). Psuedo-random sequences and arrays. *Proceedings of the Institute of Electrical and Electronic Engineers, 35*(3), 145 160.

Marmarelis, P., & Marmarelis, V. (1978). *Analysis of physiological systems*. New York, NY: Plenum Press.

Marmor, M., Hood, D., Keating, D., Kondo, M., Seeliger, M., & Miyake, Y. (2003). Guidelines for basic multifocal electroretinography (mfERG). *Documenta Ophthalmologica, 106*(2), 105 115.

Marmor, M., Kellner, U., Lai, T., Lyons, J., Mieler, W., & American Academy of Ophthalmology. (2011). Revised recommendations on screening for chloroquine and hydroxychloroquine retinopathy. *Ophthalmology, 118*(2), 415 422.

Meigen, T., & Krämer, M. (2007). Optimizing electrode positions and analysis strategies for multifocal VEP recordings by ROC analysis. *Vision Research, 47*(11), 1445 1454.

Moller, A. (1983). Use of pseudorandom noise in studies of frequency selectivity: The periphery of the auditory system. *Biological Cybernetics, 47,* 95 102.

Morland, A., Hoffmann, M., Neveu, M., & Holder, G. E. (2002). Abnormal visual projection in a human albino studied with functional magnetic resonance imaging and visual evoked potentials. *Journal of Neurology, Neurosurgery and Psychiatry With Practical Neurology, 72,* 523 526.

Moschos, M., Mallias, J., Ladas, I., Theodossiadis, P., Moschou, M., & Theodossiadis, G. (2001). Multifocal ERG in retinal detachment surgery. *European Journal of Ophthalmology, 11*(3), 296 300.

Nebbioso, M., Grenga, R., & Karavitis, P. (2009). Early detection of macular changes with multifocal ERG in patients on antimalarial drug therapy. *Journal of Ocular Pharmacology and Therapeutics, 25*(3), 249 258.

Nemoto, N., Momose, K., Kiyosawa, M., Mori, H., &

Mochizuki, M. (2004). Characteristics of first and second order kernels of visually evoked potentials elicited by pseudorandom stimulation. *Documenta Ophthalmologica, 108,* 157 163.

Ng, J., Bearse, M., Schneck, M., Barez, S., & Adams, A. (2008). Local diabetic retinopathy prediction by multifocal ERG delays over 3 years. *Investigative Ophthalmology & Visual Science, 49*(4), 1622 1628. [PubMed] [Article]

Odom, J. V. (2006). Kernel analysis. In J. Heckenlively & G. Arden (Eds.), *Principles and practice of clinical electrophysiology of vision* (2nd ed., pp. 479 485). Cambridge, MA: MIT Press.

Odom, J. V., Bach, M., Brigell, M., Holder, G. E., McCulloch, D. L., Tormene, A. P., & Vaegan. (2009). ISCEV standard for clinical visual evoked potentials (2009 update). *Documenta Ophthalmologica, 120*(1), 111 119.

Onozu, H., & Yamamoto, S. (2003). Oscillatory potentials of multifocal electroretinogram retinopathy. *Documenta Ophthalmologica, 106*(3), 327 332.

Palmowski, A. (2003). Multifocal stimulation techniques in ophthalmology Current knowledge and perspectives. *Strabismus, 11*(4), 229 237.

Palmowski-Wolfe, A., Allgayer, R., Vernaleken, B., Schötzau, A., & Ruprecht, K. (2006). Slow-stimulated multifocal ERG in high- and normal-tension glaucoma. *Documenta Ophthalmologica, 112*(3), 157 168.

Palmowski-Wolfe, A., Todorova, M., Orguel, S., Flammer, J., & Brigell, M. (2007). The 'two global flash' mfERG in high and normal tension primary open-angle glaucoma. *Documenta Ophthalmologica, 114*(1), 9 19.

Park, J., Nam, W., Kim, S., Jang, S., Ohn, Y., & Park, T. (2011). Evaluation of the central macula in commotio retinae not associated with other types of traumatic retinopathy. *Korean Journal of Ophthalmology, 25*(4), 262 267.

Penrose, P., Tzekov, R., Sutter, E., Fu, A., Allen, A., Fung, W., & Oxford, K. (2003). Multifocal electroretinography evaluation for early detection of retinal dysfunction in patients taking hydroxychloroquine. *Retina, 23,* 503 512.

Pieh, C., Hoffmann, M., & Bach, M. (2005). The influence of defocus on multifocal visual evoked potentials. *Graefe's Archives of Clinical and Experimental Ophthalmology, 243*(1), 38 42.

Pott, J. W., Jansonius, N. M., & Kooijman, A. C. (2003). Chiasmal coefficient of flash and pattern visual evoked potentials for detection of chiasmal misrouting in albinism. *Documenta Ophthalmologica, 106,* 137 143.

Rao, A., Singh, A., Mukherjee, S., & Chowdhury, M. (2015). Comparing focal and global responses on multifocal electroretinogram with retinal nerve fibre layer thickness by spectral domain optical coherence tomography in glaucoma. *British Journal of Ophthalmology, 99*(4), 500 507.

Ream, N. (1967). Testing a 2-input linear system with periodic binary sequences. *Proceedings of the Institution of Electrical Engineers, 114*(2), 305 308.

Regan, D., & Spekreijse, H. (1986). Evoked potentials in vision research 1961 86. *Vision Research, 26,* 1461 1480.

Shimada, Y., Sakurai, S., Naito, K., Sugino, T., Kojima, Y., Hori, K., & Horiguchi, M. (2011). Multifocal electroretinogram and optical coherent tomography: Prediction of visual outcome after epiretinal membrane removal. *Clinical and Experimental Optometry, 94*(3), 296 301.

Srebro, R., & Wright, W. W. (1998). Visually evoked potentials to pseudorandom binary sequence stimulation. Preliminary clinical trials. *Archives of Ophthalmology, 2,* 296 298.

Stangos, A., Petropoulos, I., Pournaras, J., Zaninetti, M., Borruat, F., & Pournaras, C. (2007). Optical coherence tomography and multifocal electroretinogram findings in chronic solar retinopathy. *American Journal of Ophthalmology, 144*(1), 131 134.

Stiefelmeyer, S., Neubauer, A., Berninger, T., Arden, G., & Rudolph, G. (2004). The multifocal pattern electroretinogram in glaucoma. *Vision Research, 44*(1), 103 112.

Sutter, E. (1987). A practical non-stochastic approach to nonlinear time-domain analysis. *Advanced Methods of Physiological Systems Modelling, 1,* 303 315.

Sutter, E. (1988). Field topography of the visual evoked response. *Investigative Ophthalmology & Visual Science, 29,* 433.

Sutter, E. (2000). The interpretation of multifocal binary kernels. *Documenta Ophthalmologica, 100*(2 3), 49 75.

Sutter, E. (2001). Imaging visual function with the multifocal m-sequence technique. *Vision Research, 41,* 1241 1255.

Sutter, E., & Tran, D. (1992). The field topography of ERG components in man. The photopic luminance response. *Vision Research, 32*(3), 433 446.

Teping, C. (1981). Determination of visual acuity by

the visually evoked cortical potential. *Klinische Monatsblätter für Augenheilkunde, 179,* 169 172.

Unterlauft, J. D., & Meigen, T. (2008). Early latency in pattern-reversal and flash mfVEP. *Der Ophthalmologe, 105*(12), 1135 1141.

Vajaranant, T., Szlyk, J., Fishman, G., Gieser, J., & Seiple, W. (2002). Localized retinal dysfunction in central serous chorioretinopathy as measured using the multifocal electroretinogram. *Ophthalmology, 109,* 1243 1250.

Verdon, W. (2008). Clinical electrophysiology in quinine induced retinal toxicity. *Optometry and Vision Science, 85*(1), 17 26.

Voltera, V. (1959). *Theory of functionals and of the integral and integro-differential equations.* Mineola, NY: Dover.

Wallenten, K., Andreasson, S., & Ghosh, F. (2008). Retinal function after vitrectomy. *Retina, 28*(4), 558 563.

Wiener, N. (1958). *Nonlinear problems in random theory*. Cambridge, MA: MIT Press.

Wildberger, H., & Junghardt, A. (2002). Local visual field defects correlate with the multifocal electroretinogram (mfERG) in retinal vascular branch occlusion. *Klinische Monatsblätter für Augenheilkunde, 219,* 254 258.

Wolff, B., Bearse, M., Schneck, M., Barez, S., & Adams, A. (2010). Multifocal VEP (mfVEP) reveals abnormal neuronal delays in diabetes. *Documenta Ophthalmologica, 121*(3), 189 196.

Wu, Z., Ayton, L., Guymer, R., & Luu, C. (2014). Comparison between multifocal electroretinography and microperimetry in age-related macular degeneration. *Investigative Ophthalmology & Visual Science, 55*(10), 6431 6439. [PubMed] [Article]

Wu, Z., Ayton, L., Makeyeva, G., Guymer, R., & Luu, C. (2015). Impact of reticular pseudodrusen on microperimetry and multifocal electroretinography in intermediate age-related macular degeneration. *Investigative Ophthalmology & Visual Science, 56,* 2100 2106. [PubMed] [Article]

Xu, J., Hu, G., Huang, T., Huang, H., & Chen, B. (2006). Using multifocal ERG responses to discriminate diabetic retinopathy. *Documenta Ophthalmologica, 112*(3), 201 207.

Yavas, G., Küsbeci, T., & Inan, U. (2014). Multifocal electroretinography in subjects with age-related macular degeneration. *Documenta Ophthalmologica, 129*(3), 167 175.

Yip, Y., Ngai, J., Fok, A., Lai, R., Li, H., Lam, D., & Lai, T. (2010). Correlation between functional and anatomical assessments by multifocal electroretinography and optical coherence tomography in central serous chorioretinopathy. *Documenta Ophthalmologica, 140*(2), 193 200.

Zhang, X. (2003). Simultaneously recording local luminance responses, spatial and temporal interactions in the visual system with m-sequences. *Vision Research, 43,* 1689 1698.

Zhang, X., Hood, D. C., Chen, C. S., & Hong, J. E. (2002). A signal-to-noise analysis of multifocal VEP responses: An objective definition for poor records. *Documenta Ophthalmologica, 104*(3), 287 302.

Zhu, Y., Zhang, T., Wang, K., & Xu, G. (2014). Prognostic value of multifocal electroretinography and optical coherence tomography in eyes undergoing panretinal photocoagulation for diabetic retinopathy. *Investigative Ophthalmology & Visual Science, 55*(10), 6358 6364. [PubMed] [Article]

Zierler, N. (1959). Linear recurring sequences. *Journal of the Society for Industrial and Applied Mathematics, 7,* 31 48.

Zierler, N. (1968). On primitive trinomials (Mod 2). *Information and Control, 13,* 541 554.